Chiang Mai J. Sci. 2019; 46(6) : 1176-1190
http://epg.science.cmu.ac.th/ejournal/
Contributed Paper

Photophysical Properties of Various Substituted Thiophene-based Heterocyclic Chalcone: Experimental and DFT Studies

Nikorn Saengsuwan [a,b], Nutjarin Klinhom [a,b], Buchita Nakwanich [a,b], Suwannee Sriyab [a,b], Panida Prompinit [c], Songwut Suramitr [a,b], and Supa Hannongbua*[a,b]

[a] Department of Chemistry, Faculty of Science, Kasetsart University, Bangkok 10900, Thailand.

[b] Center for Advanced Studies in Nanotechnology and Its Applications in Chemical, Food and Agricultural Industries, KU institute for Advanced Studies, Kasetsart University, Bangkok 10900, Thailand.

[c] National Nanotechnology Center (NANOTEC), National Science and Technology Development Agency, Klong Luang, Pathumthani 12120, Thailand.

*Author for correspondence; e-mail: fscisph@ku.ac.th

Received: 20 June 2019
Revised: 31 July 2019
Accepted: 3 August 2019

Abstract

A comprehensive study of the photophysical properties of three thiophene-based heterocyclic chalcones was investigated on the basis of joint optical spectroscopic technique and quantum chemical calculations. Three thiophene-based heterocyclic chalcone derivatives with 2,4,5-methoxy (2,4,5-OMe@Chal), 2,4,6-methoxy (2,4,6-OMe@Chal) and 3,4,5-methoxy (3,4,5-OMe@Chal) as terminal groups were focused. The thiophene-based heterocyclic chalcone, 2,4,5-OMe@Chal, 2,4,6-OMe@Chal and 3,4,5-OMe@Chal were synthesized, producing in 87%, 85% and 89% yields, respectively. The photophysical properties were performed by UV-Vis absorption and fluorescence spectroscopic technique. The obtained results indicated that the position of methoxy substituent groups brings to increasing in the fluorescence quantum yield (Φ_{fluo}). All the chalcone derivatives exhibit slightly low fluorescence quantum yields (Φ_{fluo}=*0.0051-0.0518*). In addition, Density Functional Theory (DFT) at PBE0/6-311G(d,p) level were successfully used to evaluate the molecular geometries, the characteristics of the excited singlet and triplet states. The calculated results were in well agreement with the experimental data, and indicated that the low fluorescence of 2,4,6-OMe@Chal and 3,4,5-OMe@Chal is derived from, not only intersystem crossing but also internal conversion due to the proximity effect. Among the three derivatives, it was found that 2,4,5-OMe@Chal shows higher fluorescence quantum yield than the others. This work deepens the understanding of thiophene-based heterocyclic chalcone derivatives and provides novel materials for improved fluorescence efficiencies.

Keywords: thiophene-based heterocyclic chalcone, photophysical properties, DFT calculations, fluorescence sensors

1. INTRODUCTION

Recently, thermally activated delayed fluorescence (TADF) emitters have attracted much attention not only low-cost manufacture without using rare metals and potential for high electroluminescence (EL) efficiency but also triplet excitons converting to singlet excitons [1-5]. TADF materials have broken the limitation of the internal quantum efficiency for traditional fluorescence (OLEDs) whose maximum utilization of singlet excitons is 25% due to the branching ratio of the singlet and triplet excitons (1:3). Therefor, TADF materials are considered as the next generation of lighting and display devices [6-7]. For effective TADF molecules, a small energy gap (ΔE_{ST}) between the lowest singlet excited state (S_1) and the lowest triplet excited state (T_1) is important to achieve high reverse intersystem crossing (RISC) process, because the RISC rate can be represented by $K_{RISC} \approx 1/3\exp(-\Delta E_{ST}/K_BT)$ where K_B denotes the Boltzmann constant and T is temperature [8]. Thus, harvesting the non-radiative triplet excitons generated by carrier recombination at room temperature is an important issue for developing high efficient thermally activated delayed fluorescence organic light emitting diodes (TADF-OLEDs), and it is necessary to investigate the photophysical properties of TADF molecules.

Chalcones are organic compounds that have a unique functional group of a carbonyl in conjugation with a carbon-carbon double bond, which is known as enone function [9-11]. Chalcone structure has two phenyl rings, consisting of two parts called ketone and enone parts. This molecule can be prepared by an aldol condensation between benzaldehyde and acetophenone in sodium hydroxide as a catalyst. In addition, chalcones can be distributed in plants, fruits and vegetables [12]. Chalcones have many applications, involving biological activities such as antibacterial [13], antifungal [14], anti-inflammatory [15], anti-cancer [16], antimicrobial [17], antitubercular agents [18], and antiviral agents [19]. Beside their medicinal applications, the photophysical and photochemical properties of chalcone have been neglected for a long time, while of chalcone derivatives with proper electron push-pull pairs are known to be fluorescent, nonlinear optical (NLO) [20], precursors in flavonoid synthesis [21], as well as fluorescent properties [22]. Chalcone derivatives with the smart fluorescent properties were used as fluorescent dyes [23], light-emitting diodes [24], fluorescent probes [25], and fluorescent sensors [26].

Herein, we focused three experimental synthesized molecules of the thiophene-based heterocyclic chalcone, 2,4,5-OMe@Chal, 2,4,6-OMe@Chal and 3,4,5-OMe@Chal as representative molecules due to their similar structures and unique properties in previous research [20-26]. Based on the optimized structures, the optimal function of the three molecules, were identified. Furthermore, Density Functional Theory (DFT) were applied to calculate the radiative rate and the non-radiative rate from the lowest singlet excited state (S_1) to ground state (S_0) and the intersystem crossing (ISC) rate, reverse intersystem crossing (RISC) rate between lowest singlet excited state and triplet excited state (T_1) as well as the phosphorescence rate. The obtained results were especially analyzed the excited states properties and demonstrated that the additional channel between S_1 and T_1 can promote the ISC and RISC processes for 2,4,5-OMe@Chal, 2,4,6-OMe@Chal and 3,4,5-OMe@Chal. These could provide a clear guideline for molecular luminescence simulations and the design of high efficient TADF molecules.

2. MATERIALS AND METHODS

2.1 Synthesis and Characterization

2.1.1 Materials

All starting materials were purchased from Sigma Aldrich and used without further purification. All reaction solvents were not distilled before use. ^{1}H NMR spectra were recorded on a VARIAN UNITY INOVA spectrometer which operated at 400.00 MHz for ^{1}H in deuterated chloroform ($CDCl_3$) with tetra-methysilane (TMS) as an

internal reference. UV analysis was done with a Perkin Elmer Lambda 35 UV-Vis spectrophotometer, using a quartz cell with 1 cm path length. Fluorescence analysis was obtained using a Perkin Elmer Instruments LS55 fluorescence spectrophotometer.

Fluorescence quantum yields were measured using a comparative method against a quinine sulfate standard. Quinine sulfate was dissolved in 0.1 N sulfuric acid and diluted such that its absorbance was approximately 0.5 at 400 nm. The absorbance was recorded. The solution was then accurately diluted tenfold. A fluorescence emission spectrum was taken, converted to the wavenumber scale, corrected, and integrated. The fluorescence quantum yield of all compoundswere calculated according to, Equation (1).

$$\Phi_{dye} = \Phi_{ref} \frac{I_{dye} A_{ref}}{I_{ref} A_{dye}} \bullet \frac{n_{dye}^2}{n_{ref}^2} \quad (1)$$

where: Φ_{dye} is fluorescence quantum yield of the reference (quinine sulfate; 0.55) sample in ethanol, A_{dye} and A_{ref} are the absorbances of the dye and the reference at the excitation wavelength (400 nm). I_{dye} and I_{ref} are the integrated emission intensity for the dye and reference samples. The n_{dye} and n_{ref} are the refractive indexes of the solvent use for the dye and the reference, respectively.

2.1.2 General synthesis of the thiophene-based heterocyclic chalcone derivatives

All compounds as shown in **Figure 1** have been synthesized following the procedures described herein. The thiophene-based heterocyclic chalcone derivatives, 2,4,5-OMe@Chal, 2,4,6-OMe@Chal and 3,4,5-OMe@Chal were prepared through the condensation of 2-acethylthiophene (2 mmol) with 2,4,5-trimethoxybenzaldehyde, 2,4,6-trimethoxybenzaldehyde and 3,4,5-trimethoxybenzaldehyde (2 mmol), respectively. The reactions were performed in dichloromethane (10 ml) and stirred and refluxed for 4 h in an ice bath at 5 °C. The resulting solid was collected by filtration, washed with distilled water and dried to give an amorphous yellow-coloured solid.

(*E*)-1-(2-thienyl)-3-(2,4,5-trimethoxyphenyl)-prop-2-en-1-one, (2,4,5-OMe@Chal)

The product of 2,4,5-OMe@Chal as a dark yellow powder (% yield = 87) and melting point as 129 °C. ^{1}H NMR ($CDCl_3$), δ: 8.12 (d, 1H, J = 15.6 Hz, H_{trans}), δ: 7.86 (dd, 1H, J = 0.9 Hz, J = 3.9 Hz, H_{th}), δ: 7.65 (dd, 1H, J = 0.9 Hz, J = 4.8 Hz, H_{th}), δ: 7.39 (d, 1H, J = 15.6 Hz, H_{trans}), δ: 7.17 (t, 1H, J = 3.9 Hz, H_{th}), δ: 7.12–6.53 (2H, s, H_{ar}), δ: 3.95–3.91 (9H, s, OCH_3). UV-Vis (CH_3CN) λ_{max}: 393 nm, λ_{Flu}: 526 nm.

(E)-1-(2-thienyl)-3-(2,4,6-trimethoxyphenyl)-prop-2-en-1-one, (2,4,6-OMe@Chal)

The product of 2,4,6-OMe@Chal as a yellow powder (% yield = 85) and melting point as 102 °C. ^{1}H NMR ($CDCl_3$), δ: 8.28 (d, 1H, J = 15.6, H_{trans}), δ: 7.81 (d, 1H, J = 5.1 Hz, H_{th}), δ: 7.79 (d, 1H, J = 15.6, H_{trans}), δ: 7.60 (d, 1H, J = 5.1 Hz, H_{th}), δ: 7.15 (t, 1H, J = 5.1 Hz, H_{th}), δ: 6.14 (s, 2H, H_{ar}), δ: 3.92–3.86 (9H, s, OCH_3). UV-Vis (CH_3CN) λ_{max}: 356 nm, λ_{Flu}: 462 nm.

(E)-1-(2-thienyl)-3-(3,4,5-trimethoxyphenyl)-prop-2-en-1-one, (3,4,5-OMe@Chal)

The product of 3,4,5-OMe@Chal as a pale yellow powder (% yield = 89) and melting point as 156 °C. ^{1}H NMR ($CDCl_3$), δ: 7.90 (dd, 1H, J = 0.9 Hz, J = 3.9 Hz, H_{th}), δ: 7.79 (d, 1H, J = 15.6 Hz, H_{trans}), δ: 7.70 (dd, 1H, J = 0.9 Hz, J = 3.9 Hz, H_{th}), δ: 7.32 (d, 1H, J = 15.6 Hz, H_{trans}), δ: 7.21 (t, 1H, J = 3.9 Hz, H_{th}), δ: 6.88 (s, 2H, H_{ar}), 3.95–3.92 (9H, s, OCH_3). UV-Vis (CH_3CN) λ_{max}: 344 nm, λ_{Flu}: 504 nm.

2.2 Computational Details

The ground and excited state structures of all molecules under investigation were fully optimized at the PBE0 level of theory, employing the 6-311G(d,p) basis set and were characterized as the true minima on the harmonic potential energy

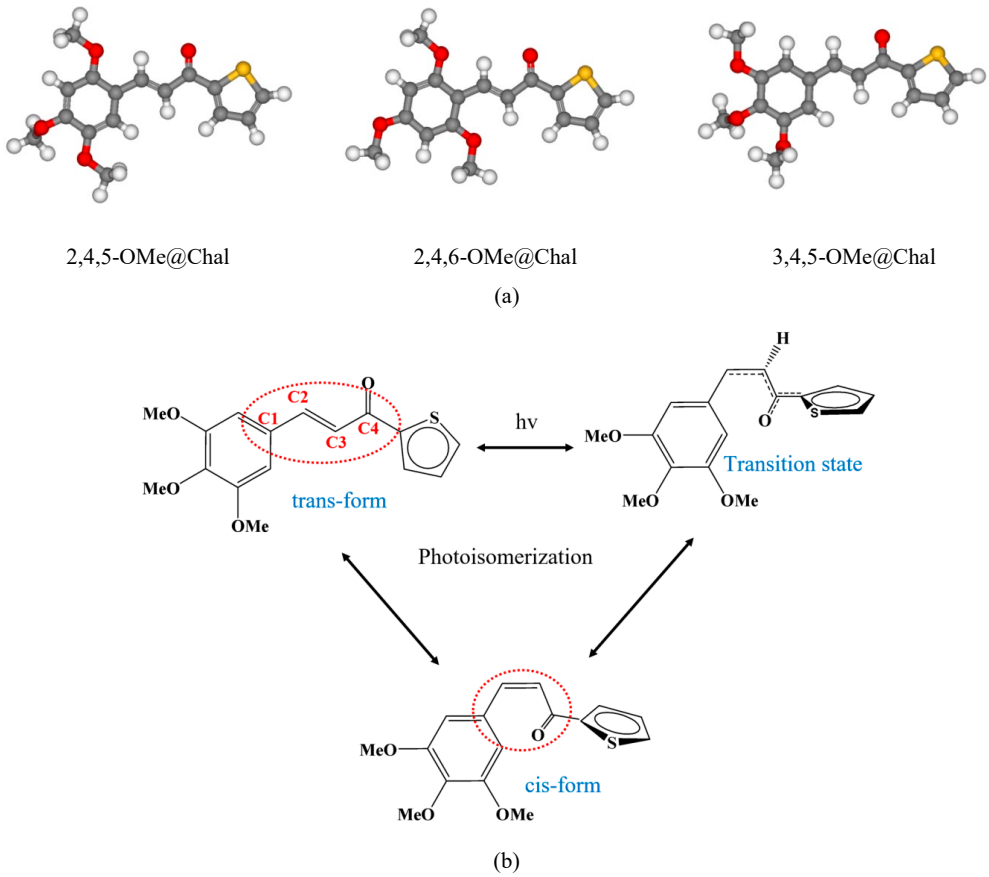

Figure 1 (a) Molecular structure of thiophene-based heterocyclic chalcone with 2,4,5-methoxy (2,4,5-OMe@Chal), 2,4,6-methoxy (2,4,6-OMe@Chal) and 3,4,5-methoxy (3,4,5-OMe@Chal) (b) Photoisomerization of 2,4,5-OMe@Chal: trans isomer, transition state and cis isomer.

hypersurfaces. To obtain the fluorescence energies (E_{Flu}), the first excited-state geometries were fully optimized by using the Time-dependent DFT method, employing the same exchange correlation functional and basis set as was used in the ground state structure optimization. The Time Dependent Density Function Theory (DFT) method with the 6-311G(d,p) basis set was applied to get excitation energies (E_{max}), and electronic transition of molecules. Structures of the first electronic excited state (S_1) were optimized by the TD-PBE0 approach [27-28] with 6-311G(d,p) basis set. In addition, the absorption spectra was also explored by the TD-PBE0/6-311G(d,p) calculations under the S_0 and S_1 minimum structures, respectively. Solvent effects were simulated by employing a polarizable continuum model (PCM) [29-30] of dichloromethane. All calculations were carried out using the Gaussian 09 program [31].

3. Results and Discussion

3.1 Photophysical Properties

The thiophene-based heterocyclic chalcone derivatives, 2,4,5-OMe@Chal, 2,4,6-OMe@Chal and 3,4,5-OMe@Chal were synthesized with the good % yield for 87, 85 and 89, respectively. The UV-Vis absorption and fluorescence spectra of compounds 2,4,5-OMe@Chal, 2,4,6-OMe@Chal and 3,4,5-OMe@Chal in acetone, acetonitrile, dimethylformamide (DMF), dimethyl sulfoxide

(DMSO), ethyl acetate and ethanol are shown in **Figure 2** and **Table 1**. All the thiophene-based heterocyclic chalcone derivatives exhibited two evident absorption bands, the first absorption band at the shorter wavelength about 324-335 nm were attributed to the UV cut-off wavelength of acetonitrile solvent that assigned to the π⟶π* transition of the π-conjugated backbone (**Figure 2**). The second band at the longer wavelength at 393, 356 and 344 nm, for 2,4,5-OMe@Chal, 2,4,6-OMe@Chal and 3,4,5-OMe@Chal, respectively, was assigned to the typical π⟶π* transition, which was obtained during electronic transition from the ground state to the intramolecular charge

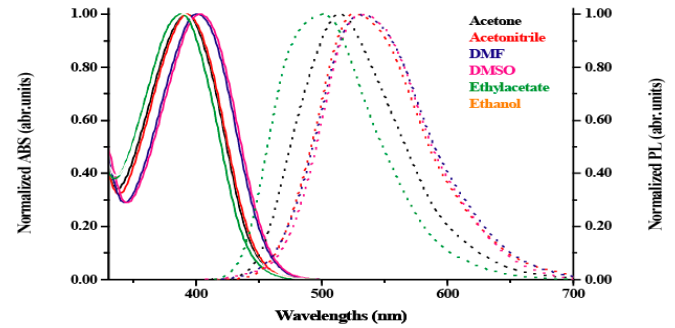

(a)

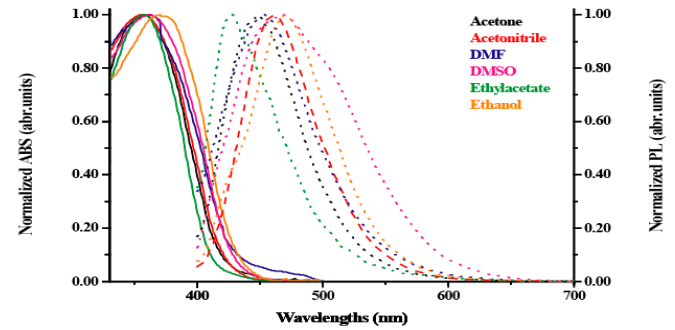

(b)

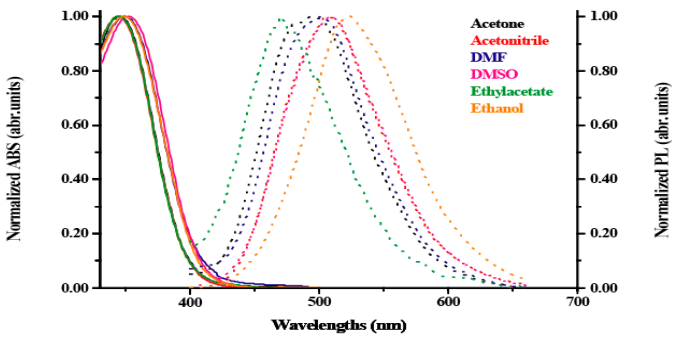

(c)

Figure 2 Absorption spectroscopy and emission spectroscopy of thiophene-based heterocyclic chalcone with (a) 2,4,5-OMe@Chal, (b) 2,4,6-OMe@Chal and (c) 3,4,5-OMe@Chal.

Table 1 Experimental determined optical properties absorption wavelength, λ_{abs} and absorption energy, E_{abs}, molar extinction coefficient, ε, emission wavelength, λ_{flu} and emission energy, E_{flu}, fluorescence quantum yield, Φ_{flu} and Stokes shift of 2,4,5-OMe@Chal, 2,4,6-OMe@Chal and 3,4,5-OMe@Chal measured in acetonitrile solution.

Compounds	λ_{abs}[nm] (E_{abs} [eV])	ε [$M^{-1}.cm^{-1}$]	λ_{flu} [nm] (E_{flu} [eV])	Φ_{flu}	Stokes shift [nm]
2,4,5-OMe@Chal	393 (3.16)	0.0158	526 (2.36)	0.0518	133
2,4,6-OMe@Chal	356 (3.48)	0.0108	462 (2.68)	0.0051	106
3,4,5-OMe@Chal	344 (3.61)	0.0120	504 (2.46)	0.0177	160

transfer (ICT) state. It shown that 2,4,5-OMe@Chal and 3,4,5-OMe@Chal exhibited considerably enhanced intramolecular charge transfer (ICT) absorption, compared to their 2,4,6-OMe@Chal. With the change of solvent polarity, the maximum absorption undergoes a small range of the movement, which can be ascribed to the intramolecular charge transfer (ICT) of 2,4,5-OMe@Chal, 2,4,6-OMe@Chal and 3,4,5-OMe@Chal. As for the photoluminescence (PL) spectra, an interesting phenomenon which is different from the traditional one has been observed. As illustrated in **Figure 2**, the emission peaks of 2,4,5-OMe@Chal, 2,4,6-OMe@Chal and 3,4,5-OMe@Chal show a large range of red shift from 450 to 530 nm with the increase of solvent polarity from acetone to ethanol. Moreover, the fluorescence emission of compounds 2,4,5-OMe@Chal, 2,4,6-OMe@Chal and 3,4,5-OMe@Chal is very weak, so that, it is hardly to be observed even under strong UV-Vis irradiation. The UV-Vis absorption spectra of the resulting 2,4,5-OMe@Chal, 2,4,6-OMe@Chal and 3,4,5-OMe@Chal in acetonitrile solution are illustrated in **Table 1**, showing the effect of the substituent on different position of phenyl group with respect to the conjugated connectivity of the methoxy substituents. The almost fluorescence emission of 2,4,5-OMe@Chal, 2,4,6-OMe@Chal and 3,4,5-OMe@Chal in acetonitrile are possible for an indication of the significant solvent relaxation in the excited state because of the twisted intramolecular charge transfer (TICT) phenomena, which mainly weakens the fluorescence emission of the compound due to its non-radiative decay. Generally, when the $\pi \rightarrow \pi^*$ transition occurs, the excited state has a larger polarity than the ground state, which leads to a greatest stabilizing effect of solvent polarity on the excited state. As a result, the emission peak moves toward the long wavelength with the increase of solvent polarity. However, if the polarity is too large, it is possible to result in the formation of the twisted intramolecular charge transfer (TICT) state, leading to the color shift and fluorescence quenching, which has been described in details by other researchers [32-39]. The solvatochromic effect on fluorescence emission of 2,4,5-OMe@Chal, 2,4,6-OMe@Chal and 3,4,5-OMe@Chal can be further evaluated by the relationship between the solvent polarity parameter (Δf) and Stokes shift of the absorption and emission maxima (Lippert-Mataga equation) [40-42]. The detailed photophysical data are presented in **Figure 3**. As depicted, 2,4,5-OMe@Chal, 2,4,6-OMe@Chal and 3,4,5-OMe@Chal exhibits large Stokes shift which gradually increases with the increase of solvent polarity. It is clearly that the slope of the fitting line for 2,4,5-OMe@Chal, 2,4,6-OMe@Chal and 3,4,5-OMe@Chal reaches a high level of -448,135, -155,108 and 358,279, respectively, which also shows obvious solvatochromic effect.

Next, we evaluated the photoluminescence properties of the thiophene-based heterocyclic chalcone derivatives. The photoluminescence

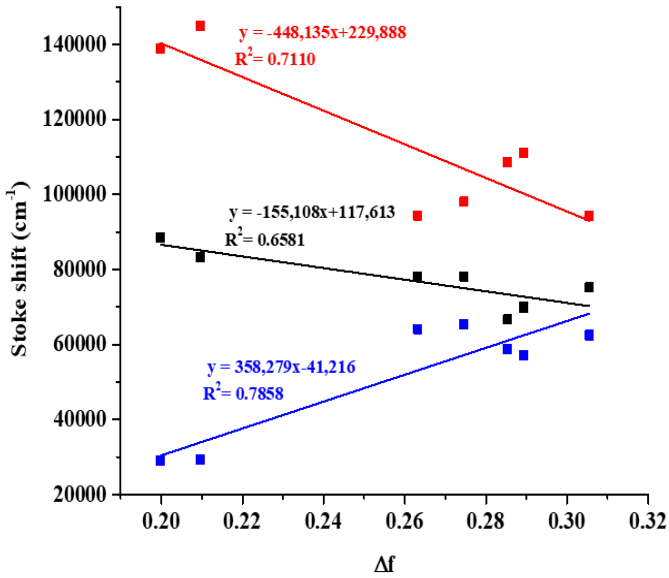

Figure 3. Variation in the Stokes shift of the 2,4,5-OMe@Chal (red), 2,4,6-OMe@Chal (black) and 3,4,5-OMe@Chal (blue) in solution with the solvent polarity parameter (Δf).

spectra of the molecules are given in **Figure 2** and **Table 1**. These are located in the blue region with emission maxima at 526, 462 and 504 nm, respectively. In **Table 1** it can be seen that the methoxy groups on the different position of phenyl ring led to large a stokes shift about 100-160 nm of emission maxima for 2,4,5-OMe@Chal, 2,4,6-OMe@Chal and 3,4,5-OMe@Chal. From the fluorescence spectra of thiophene-based heterocyclic chalcone derivatives, it was clear that as the 2,4,5 position effect of substituents increases a strong red shift of about 30 nm (λ_{Flu}; 2,4,5-OMe@Chal 526 nm and λ_{Flu}; 3,4,5-OMe@Chal 504 nm) was observed with a corresponding increase in both the fluorescence intensity and the quantum yield (**Table 1**).

The experimental fluorescence quantum yields (Φ_{flu}) were collected in **Table 1**. The maximum wavelength of the emission spectra of 2,4,5-OMe@Chal was 526 nm (Φ_{flu} = 0.0518). Whereas, 2,4,6-OMe@Chal and 3,4,5-OMe@Chal with substituted methoxy groups in phenyl ring in the emission spectra are 462 nm (Φ_{flu} = 0.0051) and 504 nm (Φ_{flu} = 0.0177), respectively. The fluorescence quantum yield of 2,4,5-OMe@Chal, 2,4,6-OMe@Chal and 3,4,5-OMe@Chal showed low fluorescence quantum yields. The stokes shift observed demonstrates that the structures of 2,4,5-OMe@Chal, 2,4,6-OMe@Chal and 3,4,5-OMe@Chal are more relaxed upon excitation and the results in a longer radiative lifetime.

3.2 Theoretical Study

Quantum chemical calculations can help to understand the photophysical behaviors and to correctly assign the transitions of the thiophene-based heterocyclic chalcone when it attached by the electron-donating groups. Moreover, computational studies allow us to systematically take into account the influence of different substituent positions on the spectroscopic features, as well as the behavior of the photophysical properties of thiophene-based heterocyclic chalcone derivatives. In order to investigate the photophysical properties of the thiophene-based heterocyclic chalcone derivatives, we investigated the excited-state electronic structure of the compound with the TD-DFT methods. Excitation energies and oscillator strengths for

the transition from the ground state S_0 to S_1, S_2 and S_3 states of the thiophene-based heterocyclic chalcone derivatives were calculated using the TD-DFT (TD-PBE0/6-311G(d,p)) method.

3.2.1 TD-DFT calculated photophysical properties of the thiophene-based heterocyclic chalcone derivatives

The absorption wavelengths, oscillator strengths and excitation character of 2,4,5-OMe@Chal, 2,4,6-OMe@Chal and 3,4,5-OMe@Chal molecules are listed in **Table 2**, together with the experimental absorption spectra. The calculated data for 2,4,5-OMe@Chal, 2,4,6-OMe@Chal and 3,4,5-OMe@Chal have the same variation trend with the experimental results. Calculations of electronic transition lead to two important transitions in the ranges 350-400 nm and 300-330 nm. We interpreted the first main peak as corresponding to the peak measured at around 350-400 nm as corresponding to the peak assigned to the $\pi \rightarrow \pi^*$ transitions. As shown in **Table 2** for the 2,4,5-OMe@Chal, 2,4,6-OMe@Chal and 3,4,5-OMe@Chal molecules possess two singlet states, the first peak 367-388 nm as the $S_0 \rightarrow S_1$ excitation and the second peak 318-332 nm as $S_0 \rightarrow S_3$ excitation that corresponding to electron transitions from HOMO→LUMO and HOMO-1→LUMO, respectively (**Figure 4**).

For 2,4,5-OMe@Chal and 3,4,5-OMe@Chal, the $S_0 \rightarrow S_1$ transition was found with an excitation energy of 388 and 367 nm and an small oscillator strength of 2,4,5-OMe@Chal (f=0.689) and 3,4,5-OMe@Chal (f=0.621). Furthermore, the $S_0 \rightarrow S_3$ excited states have absorptions about 318 nm and 331 nm and their absorption intensities are almost the same (f=0.279 and f=0.284) for 2,4,5-OMe@Chal and 3,4,5-OMe@Chal, respectively. In contrast to the case of 2,4,6-OMe@Chal, a fully allowed $S_0 \rightarrow S_1$ transition was found with excitation energy of 380 nm with high oscillator strength f=0.921 and the 332 nm with low oscillator strength f=0.035 for the $S_0 \rightarrow S_3$ excitation.

For the 2,4,5-OMe@Chal, 2,4,6-OMe@Chal and 3,4,5-OMe@Chal, the electron transitions from HOMO→LUMO and HOMO-1→LUMO are dominant in the configurations of the state transition of 367-388 nm and 318-332 nm, respectively. The bathochromic shifts in absorption of 2,4,5-OMe@Chal, as compared to 2,4,6-OMe@

Table 2 Excitation energies, oscillator strengths (f), composition of orbitals, and absorption wavelength of the 2,4,5-OMe@Chal, 2,4,6-OMe@Chal and 3,4,5-OMe@Chal.

State	eV	nm	f	Composition	Expt.(nm)
	2,4,5-OMe@Chal				
$S_0 \rightarrow S_1$	3.19	388	0.6892	HOMO→LUMO (92%)	393
$S_0 \rightarrow S_2$	3.55	349	0.0001	H-4→LUMO (85%)	-
$S_0 \rightarrow S_3$	3.89	318	0.2792	H-1→LUMO (82%)	-
	2,4,6-OMe@Chal				
$S_0 \rightarrow S_1$	3.26	380	0.9210	HOMO→LUMO (94%)	356
$S_0 \rightarrow S_2$	3.60	345	0.0000	H-4→LUMO (87%)	-
$S_0 \rightarrow S_3$	3.73	332	0.0347	H-1→LUMO (78%)	-
	3,4,5-OMe@Chal				
$S_0 \rightarrow S_1$	3.37	367	0.6211	HOMO→LUMO (91%)	344
$S_0 \rightarrow S_2$	3.55	349	0.0000	H-5→LUMO (86%)	-
$S_0 \rightarrow S_3$	3.74	331	0.2839	H-1→LUMO (85%)	-

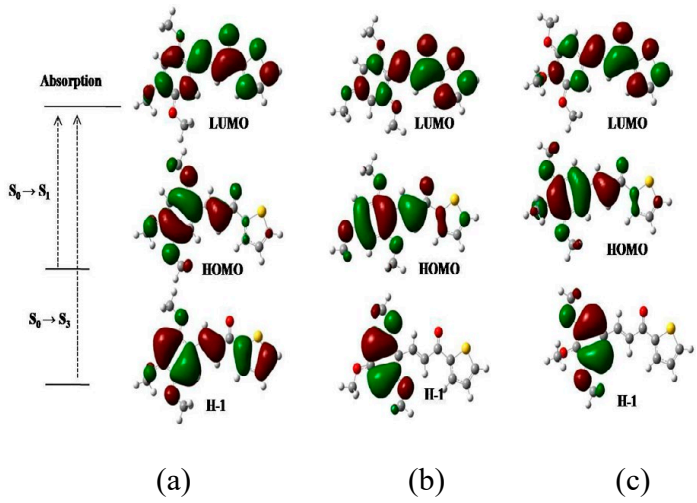

Figure 4. Electronic transition of (a) 2,4,5-OMe@Chal, (b) 2,4,6-OMe@Chal and (c) 3,4,5-OMe@Chal molecules.

Chal and 3,4,5-OMe@Chal, are presumably due to the 2,4,5 position are effective more than 2,4,6 and 3,4,5 positions. As a result of the increase in electron-donating ability of the methoxy group attached at the 2,4,5-positions of phenyl group 2,4,5-OMe@Chal, the ICT absorption peaks were significantly red-shifted to be 388 nm as found from calculations and experimental results (**Table 2**). This indicates that 2,4,5-OMe@Chal induced more effective ICT interaction from electron-donating conjugated on the phenyl ring to thiophene ring. The results indicate that the positions of substituent of electron-donating abilities are effect to electronic properties when the substituents as the methoxy groups changed from position 2 to position 6 of the phenyl ring. The calculated wavelengths of 2,4,5-OMe@Chal, 2,4,6-OMe@Chal and 3,4,5-OMe@Chal (388, 380 and 367 nm, respectively) agree well with the experimental spectra (393, 356 and 344 nm) in acetonitrile solution.

The molecular orbitals relevant for the 2,4,5-OMe@Chal, 2,4,6-OMe@Chal and 3,4,5-OMe-@Chal molecules are presented in **Figure 4**. The molecular orbitals show that the transition from HOMO (highest-occupied molecular orbital) to LUMO (lowest-unoccupied molecular orbital) is clearly indicates a complete transfer of charge from the phenyl ring to the thiophene ring and the transition from HOMO to LUMO is assigned to the $\pi \rightarrow \pi^*$ transition. The electron density distribution in all these orbitals confirms ICT and the $\pi \rightarrow \pi^*$ transition of electronic absorption for 2,4,5-OMe@Chal, 2,4,6-OMe@Chal and 3,4,5-OMe@Chal as mentioned in this section. A comparison of 2,4,5-OMe@Chal, 2,4,6-OMe@Chal and 3,4,5-OMe@Chal reveals how the different phenyl substituents give rise to differences in the optical properties. The most probable transitions of all compounds, which account from the highest oscillator strength, are considered in **Table 2**. The oscillator strength (*f*) of 2,4,5-OMe@Chal, 2,4,6-OMe@Chal and 3,4,5-OMe@Chal are 0.689, 0.921 and 0.621, respectively, corresponding to $S_0 \rightarrow S_1$ (HOMO→LUMO) transition at 388, 380 and 367 nm, respectively, whereas, the $S_0 \rightarrow S_3$ (HOMO-1→LUMO) transition are 318 nm (f=0.279), 332 nm (f=0.035) and 331 nm (f=0.284), respectively. It is indicated that the main transition of 2,4,6-OMe@Chal has the larger oscillator strength as the most probable ICT transition more than $\pi \rightarrow \pi^*$ transition from ground state to excited

state. These results suggested that the effective position of substituents play an important role on electronic properties on the phenyl ring of thiophene-based heterocyclic chalcone derivatives.

3.2.2 Photoisomerization dynamic mechanism

To examine the nature of photo-isomerization insight the molecule, the S_0 and S_1 energy profiles along the dihedral angles (θ=C1-C2-C3-C4) to twisting around C2-C3 bond were investigated as shown in **Figure 5**.

The potential curves (PECs) of the S_0 (red line) an S_1 states (blue line) were determined starting from θ=0° to θ=180° of the dihedral angles. The PECs have been determined on the basis of the DFT and TD-DFT using PBE0/6-311G(d,p) level of theory in acetonitrile solution at their optimized geometries. The PEC of the ground state (red line) clearly showed that the 2,4,5-OMe@Chal in trans form was more stable than cis one because it required less energy than the cis form. For the PEC of excited state (blue line), the cis form became more stable than the trans form because the planar cis-type structure presented above the global minimum of the excited state. As the C-C torsional angles increased from 0° to 90°, the PEC of S_1 decreased while the PEC of S_0 increased and both reached $S_1 \rightarrow S_0$ intersection at θ=C1-C2-C3-C4=90°. After the presence of conical intersection, a back twist form to cis form could occur and this led to the presence of only cis form of molecules at the end of reaction coordinate. Thus, based on our calculated results, it could be remarked that the conical intersection between S_1 and S_0 potential energy surfaces played the most important role in nonradiative deactivation of the dye via ultrafast internal conversion of the excited system to the ground state. The trans*→cis* transformation could occur in the excited state through a barrier-less path because of no energy barrier in the S_1 excited state. The results in an emergence of a very large Stokes shift during an emission. After decaying to the ground state, the photoisomerization (cis form) reverted to the original trans form via the barrier for reverse isomerization. This result implied that the presence of ground state to convert from trans→cis was more difficult than that of the reverse isomerization process from cis→trans, where it was high favorable for excited state occurrence. The ground state process was possible to occur when applying thermal treatment

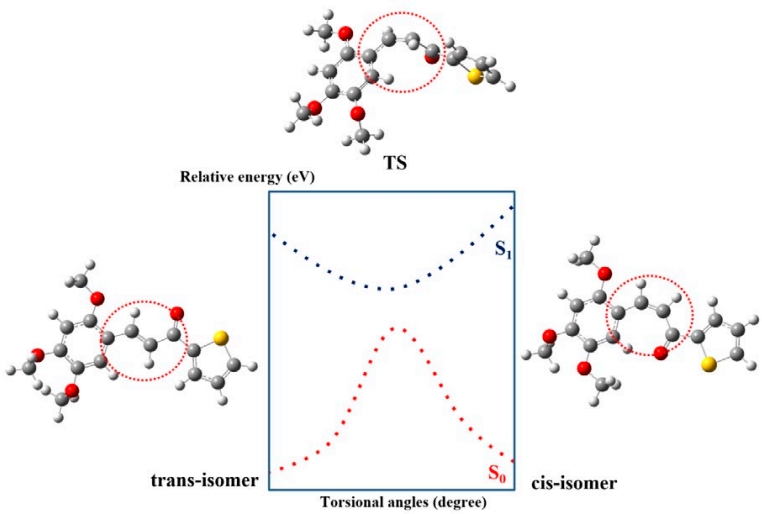

Figure 5. Potential energy curves (PECs) of the state S_0 and S_1 relevant in the photoisomerization of 2,4,5-OMe@Chal molecule.

to the dye for reduce the energy barrier to the process. From the evidences, it suggested that the ground state process was inoperative, while the excited state process was feasible in the dye molecule.

As mentioned above, the results of all the calculations show the photoiosomerization properties, trans to cis isomers, of 2,4,5-OMe@Chal, 2,4,6-OMe@Chal and 3,4,5-OMe@Chal depend on the relative position between the S_0 and S_1 transition states. Based on the optimized structures, we identify the optimal functional for 2,4,5-OMe@Chal, 2,4,6-OMe@Chal and 3,4,5-OMe@Chal. Furthermore, we calculate the radiative rate (k_r), nonradiative rate (k_{nr}) from lowest singlet excited state (S_1) to ground state (S_0) and the intersystem crossing (ISC) rate (k_{isc}), reverse intersystem crossing (RISC) rate (k_{risc}) between lowest singlet excited state (S_1) and triplet excited state (T_1) as well as the phosphorescence rate (k_{phos}). Through our calculation, we analyze the excited states properties and demonstrate that the additional channel between S_1 and T_1 can promote the ISC and RISC processes for 2,4,5-OMe@Chal, 2,4,6-OMe@Chal and 3,4,5-OMe@Chal. This could provide a clear guidance for molecular luminescence simulations and the design of high efficient molecules. In addition, the radiative lifetime (τ), radiative (k_r) and nonradiative (k_{nr}) rate constants were considered to describe the relaxation processes in the excited states. The emission calculations were performed by vertical de-excitation of 2,4,5-OMe@Chal, 2,4,6-OMe@Chal and 3,4,5-OMe@Chal using the PBE0/6-311G(d,p) method in their first singlet excited state (S_1). This was followed TD-DFT calculations employing the TD-PBE0/6-311G(d,p) method from the singlet ground state (S_0) using the former geometries. The fluorescence transition energies (E_{Flu}) and oscillator strengths (f) were used to calculate the radiative lifetime (τ) using the Einstein transition probabilities according to the following formula,

$$\tau = \frac{c^2}{2(E_{Flu})^2 f} \quad (2)$$

Where c is the velocity of light, E_{Flu} is the fluorescence transition energy, and f is the oscillator strength.

Based on the radiative (k_r) and nonradiative (k_{nr}) rate constants have been calculated according to Equation (3) and (4).

$$k_{tot} = \frac{1}{\tau} = k_r + k_{nr} \quad (3)$$

$$k_r = \frac{\Phi_{flu}}{\tau} \quad (4)$$

The predicted emission energies (E_{flu}), radiative lifetime (τ) and the rate constants (k_{tot}, k_r and k_{nr}) are summarized in **Table 3**. The results indicate that the calculated fluorescence of 2,4,5-OMe@Chal, 2,4,6-OMe@Chal and 3,4,5-OMe@Chal molecule exhibit 517, 438 and 459 nm, respectively for S_1 with the largest oscillator strength arising from HOMO→LUMO corresponding to π→π* excitation. Again, the results are in agreement with the experimental results of 526, 462 and 504 nm. The result shows that the radiative lifetimes (τ) of the 2,4,6-OMe@Chal and 3,4,5-OMe@Chal are shorter than those of the 2,4,5-OMe@Chal. This indicates that the emission or fluorescence of 2,4,5-OMe@Chal, 2,4,6-OMe@Chal and 3,4,5-OMe@Chal are complete following geometry relaxation subsequent to the photo-excitation and also nonradiative decay to the ground state. This means the radiative and nonradiative decay is different between the compounds. The radiative (k_r) and nonradiative (k_{nr}) rate constants are more dominant for 2,4,5-OMe@Chal, 2,4,6-OMe@Chal and 3,4,5-OMe@Chal. It shows that both the radiative and nonradiative de-excitation rates are affected by the position substituent groups; with the 2,4,5-position giving a radiative rate enhancement. As discussed earlier, the radiative lifetime is dependent on their position.

In organic semiconductors, the triplet exciton state usually lies below the singlet exciton state,

Table 3 Wavelength of emission energies, radiative lifetime (τ), radiative rate (k_r), nonradiative rate (k_{nr}) and singlet-triplet energy splitting (ΔE_{ST}) using PCM-TD-PBE0/6-311G(d,p) method in acetonitrile solution for the 2,4,5-OMe@Chal, 2,4,6-OMe@Chal and 3,4,5-OMe@Chal.

Compounds	E_{Flu} (nm)	τ (ns)	k_r (10^9 s^{-1})	k_{nr} (10^9 s^{-1})	k_{tot} (10^9 s^{-1})	ΔE_{ST} (eV)
trans-isomer						
2,4,5-OMe@Chal	517	6.75	0.0077	0.1405	0.1481	0.93
2,4,6-OMe@Chal	438	2.63	0.0019	0.3783	0.3802	1.21
3,4,5-OMe@Chal	459	3.36	0.0053	0.2923	0.2976	1.30
cis-isomer						
2,4,5-OMe@Chal	533	7.96	0.0065	0.1191	0.0546	0.78
2,4,6-OMe@Chal	421	2.56	0.0020	0.3886	0.0051	0.17
3,4,5-OMe@Chal	470	7.62	0.0023	0.1289	0.0181	0.35

and the singlet state can be directly excited by the absorption of a photon. The excited electron gets transferred to the corresponding vibrational energy of the triplet state and its spin gets flipped due to the spin-orbit interaction. Hence, a singlet exciton gets converted to a triplet and the mechanism is called intersystem crossing (ISC) and reverse intersystem crossing (RISC). Traditionally, the photoluminescence properties of aromatic carbonyl compounds have been interpreted based on intersystem crossing due to the $n \rightarrow \pi^*$ transition state and have been developed in the electron transfer reaction by using such characteristics; however, internal conversion due to the proximity effect is currently being recognized in various studies in which most compounds are carbonyl derivatives. This effect is also considered important when developing emission materials. In **Table 3**, we give a detailed summary of the photoluminescence properties and processes of 2,4,5-OMe@Chal, 2,4,6-OMe@Chal and 3,4,5-OMe@Chal. In addition, the specific fluorescence behaviors of thiophene-based heterocyclic chalcone derivatives, which we measured using the same methods, are also described there; that is, with this work, we can also systematize the photophysical and photoluminescence properties of thiophene-based heterocylclic chalcone derivatives. Further, this classification suggests the possibility that the photoluminescence properties of the chalcone derivatives may be predictable by using TD-DFT calculations. Most importantly, a small $\measuredangle E_{ST}$ is critical to activate the reverse intersystem crossing (RISC) process from T_1 to S_1. The ΔE_{ST} values of 2,4,5-OMe@Chal, 2,4,6-OMe@Chal and 3,4,5-OMe@Chal are listed in **Table 3**. As expected from the frontier orbitals analysis, the $\measuredangle E_{ST}$ values of 2,4,5-OMe@Chal is very small, indicating that they plausibly has 2,4,5-OMe@Chal properties with efficient up-conversion from T_1 to S_1. In details, 2,4,6-OMe@Chal and 3,4,5-OMe@Chal have the same ΔE_{ST}, while 2,4,5-OMe@Chal possesses a slight lower $\measuredangle E_{ST}$ than 2,4,6-OMe@Chal and 3,4,5-OMe@Chal, suggesting that varying the position of the methoxy group has an influence on $\measuredangle E_{ST}$ values.

4. CONCLUSIONS

In summary, photophysical properties for photoisomerization of the chalcone-based heterocyclic derivatives have been successfully investigated using experimental methods combined with theoretical calculations. We present here the effect of different position of methoxy substituent

groups to photophysical properties of chalcone. The studies of structural properties show the methoxy group effect to the phenyl ring but no effect to the enone linkage. The dynamics of the photoisomerization of trans to cis isomers were considered based on the potential energy curves of the S_1 along the proton transfer coordinate. The trans form was high stable, while the cis form was mainly existed solutions. It revealed that the energy barrier of the trans form was lower than that of the cis form allowing an occurrence of excited state process being more rapidly and easily than that of the cis form. The conical intersection between S_1 and S_0 potential energy surfaces of the dye could lead to $\pi \rightarrow \pi^*$ character. This indicates that theoretical studies based on density functional theory calculations can help clarify the role of charge transfer of the chalcone-based hetrocyclic chalcone derivatives. The introduction of electron-donating into methoxy based derivatives could prove very useful in the development of materials with improved fluorescence efficiencies. The information about low fluorescence compounds dominated by both intersystem crossing and internal conversion has been important in the fields of probe, sensors, and electron transfer reactions, as has that about high fluorescence compounds. We believe this knowledge will facilitate the design of not only emitting materials but also other applications.

Acknowledgements

This work is partially supported by grants from Kasetsart University, the Thailand Research Fund (RTA5380010 to SH and MRG5480273 to SS). NS was supported from the Asea-Uninet, the University of Vienna and Science Research Fund (ScRF), the Commission on Higher Education (a scholarship to NS), Center of Nanotechnology Kasetsart University, Kasetsart University Research and Development Institute (KURDI), National Nanotechnology Center (NANOTEC), the Center for Advanced Studies in Nanotechnology and Its Applications in Chemical, Food and Agricultural Industries, the National Electronics and Computer Technology Center and Faculty of Science, Kasetsart University, Ministry of Education trough "the National Research University Project of Thailand (NRU)" and the "National Center of Excellence for Petroleum, Petrochemical and Advanced Materials (NCEPPAM)" are gratefully acknowledged for research facilities. The calculations were performed in part on the Schrödinger III cluster and the VSC of the University of Vienna.

References

[1] Uoyama H., Goushi K., Shizu K., Nomura H. and Adachi C., *Nature.*, 2012; **492**: 234-238.

[2] Cui L.S., Ruan S.B., Bencheikh F., Nagata R., Zhang L., Inada K., Nakanotani H., Liao L.S. and Adachi C., *Nat. Commun.*, 2017; **8**: 2250-2257.

[3] Zhang J., Chen W., Chen R., Liu X.K., Xiong Y., Kershaw S.V., Rogach A.L., Adachi C., Zhang X. and Lee C.S., *ChemComm*, 2016; **52**: 11744-11747.

[4] Huang J., Nie H., Zeng J., Zhuang Z., Gan S., Cai Y., Guo J., Su S.J., Zhao Z. and Tang B.Z., *Angew. Chem.*, 2017; **129**: 13151-13156.

[5] Liu M., Komatsu R., Cai X., Sasabe H., Kamata T., Nakao K., Liu K., Su S.J. and Kido J., *Adv. Opt. Mater.*, 2017; **5**: 1700334(1)-34(8).

[6] Zhang Y., Zhang D., Cai M., Li Y., Qiu Y. and Duan L., *Nanotechnology*, 2016; **27**: 94001-94008.

[7] Kawasumi K., Wu T., Zhu T., Chae H.S., VanVoorhis T., Baldo M.A. and Swager T.M., *J. Am. Chem. Soc.*, 2015; **137**: 11908-11911.

[8] Dias F.B., Penfold T.J., Monkman A.P., *Methods Appl. Fluores.*, 2017; **5**: 012001-25.

[9] Hsieh C.J., Xu K., Graham T.A.J., Tu Z., Dhavale D., Kotzbauer P. and Mach R.H., *ACS Omega*, 2018; **3**: 4486-4493.

[10] Reddy P.O.V., Hridhay M., Nikhil K., Khan S., Jha P.N., Shah K. and Kumar D., *Bioorg. Med. Chem. Lett.*, 2018; **28**: 1278-1282.

[11] da Costa R.G., Farias F.R.L., Back D. and Limberger J., *Tetrahedron Lett.*, 2018; **59**: 771-775.

[12] Kozlowski D., Trouillas P., Calliste C., Marsal P., Lazzaroniand R. and Duroux J., *J. Phys. Chem. A*, 2007; **111**: 1138-1145.

[13] Nielsen S.F., Boesen T., Larsen M., Schonning K. and Kromann H., *Bioorg. Med. Chem.*, 2004; **12**: 3047-3054.

[14] Batovska D., Parushev S., Slavova A., Bankova V., Tsvetkova I., Ninova M. and Najdenski H., *Eur. J. Med. Chem.*, 2007; **42**: 87-92.

[15] Won S.J., Liu C.T., Tsao L.T., Weng J.R., Ko H.H., Wang J.P. and Lin C.N., *Eur. J. Med. Chem.*, 2005; **40**: 103-112.

[16] Syam S., Abdelwahab S.I., Al-Mamary M.A. and Mohan S., *Molecules*, 2017; **17**: 6179-6195.

[17] Choudhary A. and Juyal V., *Int. J. Pharm. Pharm. Sci.*, 2011; **3**: 125-128.

[18] Lin Y.M., Zhou Y., Flavin M.T., Zhou L.M., Nie W. and Chen F.C., *Bioorg. Med. Chem.*, 2002; **10**: 2795-2802.

[19] Gan X., Hu D., Chen Z., Wang Y. and Song B., *Bioorg. Med. Chem. Lett.*, 2017; **27**: 4298-4301.

[20] Kiran M.S., Anand B., Sankara-Sai S.S. and Rao G.N., *J. Photochem. Photobiol. A*, 2014; **290**: 38-42.

[21] Petrussa E., Braidot E., Zancani M., Peresson C., Bertonili A., Patui S. and Vianello A., *Int. J. Mol. Sci.*, 2013; **14**: 14950-14973.

[22] Rurack K., Bricks J.L., Reck G., Radeglia R. and Resch-Genger U., *J. Phys. Chem. A*, 2000; **104**: 3087-3109.

[23] Suh W., Jeon H., Lee J.Y., Lim C.M., Lee S.K. and Noh D.Y., *Bull. Korean Chem. Soc.*, 2012; **33**: 443-448.

[24] Ahmed K.A., El-Molla M.M., Abdel-Mottaleb M.S.A., Mohamed S.A. and El-Saadany S., *Res. J. Chem. Sci.*, 2013; **3**: 3-18.

[25] Lee S.C., Kang N.Y., Park S.J., Yun S.W., Chandran Y. and Chang Y.T., *ChemComm*, 2012; **48**: 6681-6683.

[26] Wei Y., Qin G., Wang W., Shuang S. and Dong C., *J. Lumin.*, 2011; **131**: 1672-1676.

[27] Adamo C. and Barone V., *J. Chem. Phys.*, 1999; **110**: 6158-6170.

[28] Ernzerhof M. and Scuseria G.E., *J. Chem. Phys.*, 1999; **110**: 5029-5036.

[29] Barone V., Cossi M. and Tomasi J., *J. Chem. Phys.*, 1997; **107**: 3210-3221.

[30] Tomasi J., Mennucci B. and Cammi R., *Chem. Rev.*, 2005; **105**: 2999-3094.

[31] Frisch M.J.T., Schlegel G.W., Scuseria H.B., Robb G.E., Cheeseman M.A., Scalmani J.R., Barone G., Mennucci V., Petersson B., Nakatsuji G.A., Caricato H., Li M., Hratchian X., Izmaylov H.P., Bloino A. F., Zheng J., Sonnenberg G., Hada J. L., Ehara M., Toyota M., Fukuda K., Hasegawa R., Ishida J., Nakajima M., Honda T., Kitao Y., Nakai O., Vreven H., Montgomery T., Peralta Jr J.A., Ogliaro J.E., Bearpark F., Heyd M., Brothers J.J., Kudin E., Staroverov K.N., Keith V.N., Kobayashi T., Normand R., Raghavachari J., Rendell K., Burant A., Iyengar J.C., Tomasi S.S., Cossi J., Rega M., Millam N., Klene J.M., Knox M., Cross J.E., Bakken J.B., Adamo V., Jaramillo C., Gomperts J., Stratmann R., Yazyev R.E., Austin O., Cammi A.J., Pomelli R., Ochterski C., Martin J.W., Morokuma R.L., Zakrzewski K., Voth V.G., Salvador G.A., Dannenberg P., Dapprich J.J., Daniels S., Farkas A.D., Foresman O., Ortiz J.B., Cioslowski J.V. and Fox D.J., Gaussian 09, revision D.01, 2013.

[32] Elzupir O.A., Ibnaouf K.H., Idriss H., Ibrahem M.A., Prasad S., Alrajhi M.A.,

AlSalhi M.S. and Alaamer A.S., *Acta Phys. Pol. A*, 2018; **133**; 121-125.

[33] Ibnaouf K.H., Elzupir A.O., AlSalhi M.S., Alaamer A.S. and Abdulaziz S., *Opt. Mater.*, 2018; **76**: 216-221.

[34] Ibnaouf K.H., Ali M.K.M., Elzupir A.O., Ibrahem M.A., Idriss H., Alaamer A.S., Alrajhi M.A. and Alsalhi M.S., *Dig. J. Nanomater. Bios.*, 2017; **12**: 423-430.

[35] Gaber M., El-Daly S.A., Fayed T.A. and El-Sayed Y.S., *Opt. Laser Technol.*, 2008; **40**: 528-537.

[36] Shkir M., Muhammad S., AlFaify S., Irfan A., Patil P.S., Arora M., Algarni H. and Jingping Z., *RSC Adv.*, 2015; **5**: 87320-87332.

[37] Shkir M., Patil P.S., Arora M., AlFaify S., and Algarni H., *Spectrochim. Acta A*, 2017; **173**: 445-456.

[38] Goto Y., Hayashi A., Kimura Y. and Nakayama M., *J. Cryst. Growth*, 1991; **108**: 688-698.

[39] Ramkumar V. and Kannan P., *Opt. Mater.*, 2015; **46**: 605-613.

[40] Lakowicz J.R., *Principles of Fluorescence Spectroscopy* (2006).

[41] Lippert E., *Electrochemistry*, 1957; **61**: 962-975.

[42] Mataga N., Kaifu Y. and Koizumi M., *Bull. Chem. Soc. Jpn.*, 1956; **29**: 465-470.